

Supramolecular Polymers

Ion Mobility Mass Spectrometry to Probe Sequences in Supramolecular Copolymers

Cédric Przybylski,* Patrick Brocorens,* Laetitia-Eiko Xerri, Antoine Perennes, Geoffroy Gontard, Roberto Lazzaroni, Matthieu Raynal,* and Laurent Bouteiller*

Abstract: The analysis of the microstructure of supramolecular copolymers is difficult because of their dynamic character. Here, benzene-1,3,5-tricarboxamide (BTA) co-assemblies are analysed by ion mobility – mass spectrometry (IM–MS) to reveal the presence of various sequences. For example, the IM–MS mobilogram for hexamers composed of 4 units from a first monomer and 2 units from a second monomer is a broad distribution due to the presence of 9 possible isomeric sequences, which can be sorted out based on calculated collision cross-sections. This approach gives unprecedented information on supramolecular copolymer sequences.

Introduction

Supramolecular polymers, formed by reversible assembly of monomers, are currently developed for numerous applications, where reversibility brings desirable features such as self-healing or stimuli responsiveness.^[1–3] Supramolecular copolymers are of particular interest because their composition can be tuned by simply adding an additional monomer to a pre-existing system (unlike covalent copolymers where changing the composition requires starting the synthesis over again). In particular, some of us have demonstrated

that supramolecular copolymers can be used as an adaptable and stimuli-responsive platform for catalysis.^[4–6] For instance, it was possible to synthesize each of the four stereoisomers of a difunctional substrate in one pot and with a single catalyst whose stereoselectivity was tuned under kinetic control during the catalytic reactions.^[7] Although these achievements are unprecedented, they are limited by a lack of knowledge of the local arrangement of the monomers. Indeed, the reactivity of the catalytic centre is expected to be influenced by its direct neighbours along the supramolecular copolymer, and a control of the monomer sequences would open a new avenue for a better design of such catalysts. In fact, probing the sequences in supramolecular copolymers has consequences far beyond the field of catalysis. It is, for instance, greatly relevant in the context of electronic applications, where the copolymer microstructure directly informs on the contacts between electron-rich and electron-poor monomers.^[8] Monitoring the sequences in supramolecular copolymers is also of prime importance in the context of biological applications, where the distribution of functional monomers along the backbone can adapt and allow multitopic interactions with biomolecules such as siRNA.^[9]

In the field of covalent copolymers, the importance of controlling the sequences is well established and various approaches have been developed.^[10] In the case of supramolecular copolymers, kinetic-control has emerged as a powerful tool to steer the microstructure,^[11] and precise engineering of the nucleation event(s) allows the preparation of supramolecular block-copolymers.^[12,13] However, the control of the polymerization in these systems comes with the requirement of their lack of dynamicity, i.e. that monomer positions in the final supramolecular copolymer are frozen. Under thermodynamic control, the situation is more tricky: apart from obvious cases where alternation is enforced by the complementarity of two comonomers,^[14–16] in most cases a random arrangement of the monomers is assumed, without quantitative evaluation. This is mainly due to the limitations of analytical tools available to probe the microstructure of the supramolecular copolymers.^[17] Electron microscopy can be used, but it does not reach molecular resolution and it is limited to highly-emissive monomers or requires specific sample preparation notably to label the monomers.^[18] Spectroscopic monitoring during melting of the co-assembly (by UV/Vis absorption and CD analyses) can also be used to provide a hint of the initial copolymer microstructure.^[19] For instance, a multiblock structure has been proposed by fitting these melting curves with a two-

[*] C. Przybylski, A. Perennes, G. Gontard, M. Raynal, L. Bouteiller Sorbonne Université, CNRS, Institut Parisien de Chimie Moléculaire, IPCM, 4 place Jussieu, 75005, Paris, France
 E-mail: cedric.przybylski@univ-evry.fr
 matthieu.raynal@sorbonne-universite.fr
 laurent.bouteiller@sorbonne-universite.fr

C. Przybylski
 Université Paris-Saclay, Univ Evry, CY Cergy Paris Université, CNRS, LAMBE, 91025, Evry-Courcouronnes, France

P. Brocorens, L.-E. Xerri, R. Lazzaroni
 Service de Chimie des Matériaux Nouveaux, Institut de Recherche sur les Matériaux, Université de Mons, Place du Parc, 20, B-7000, Mons, Belgium
 E-mail: patrick.brocorens@umons.ac.be

© 2025 The Author(s). Angewandte Chemie International Edition published by Wiley-VCH GmbH. This is an open access article under the terms of the Creative Commons Attribution Non-Commercial License, which permits use, distribution and reproduction in any medium, provided the original work is properly cited and is not used for commercial purposes.

component mass balance model^[20] allowing for a numerical evaluation of the free energy of the hetero-interaction.^[8,21,22] However, as the interpretation of the copolymer microstructure is strongly dependent on the value of this (model dependent) free energy, the development of a more direct technique is highly desirable.

Ion mobility - mass spectrometry (IM-MS) performs a gas phase separation of ions according to their size and shape and yields specific collision cross-sections (CCS, Å²) that contain rich structural information.^[23] For two decades, IM-MS has fuelled a fast increase in structural studies in both chemical and biological sciences, by allowing the discrimination of isomers, and providing information on 3D conformations. IM-MS has mostly been used to separate small chemical compounds as well as to study protein conformations, foldamers,^[24] and polymers.^[25] In the case of supramolecular assemblies, electrospray, which enables a high ionization efficiency at relatively low energy input, is the preferred ionization technique, as it favours the transfer of intact assemblies from solution to the gas-phase.^[26,27] Most of the studies deal with discrete host-guest complexes,^[28] interlocked molecules,^[29] or metal-organic cages,^[30] with very few examples of supramolecular homopolymers,^[31,32] and none of supramolecular copolymers. In the present manuscript, we describe our attempt to use IM-MS to probe the sequences in supramolecular copolymers.

Results and Discussion

Selection of the Monomers and Characterization of the Assemblies in Solution and Solid State

Benzene-1,3,5-tricarboxamide (BTA) monomers **1a** (achiral) and **2a** (either enantiomers, Figure 1) have been widely used as co-monomers of a phosphine-functionalized BTA ligand to develop a versatile platform for enantioselective catalysis.^[4,33,34] We decided to combine these two monomers for the following reasons: (i) they possess C₃-symmetry which limits the number of potential conformers in the co-assembled structures; (ii) monomer **1a** forms long stacks in solution,^[34,35] which should help **2a** to co-assemble and form helical stacks, and (iii) monomer **2a** is larger than monomer **1a** thus offering the possibility to differentiate isomeric structures, such as oligomers with different sequences, thanks to their CCS. While the dodecyl chains in **1a** and **2a** are well suited for solution studies in low polarity solvents, we prepared analogues with shorter isopropyl chains (**1b** and **2b**) that are better suited for gas phase and computational studies. The nature of the alkyl chain is not expected to influence the results as long as the same alkyl chain is present on both monomers.

In their individual solutions, **1a** forms stacks (through hydrogen bonding of amide groups) and (*R*)-**2a** forms dimers (through hydrogen bonds involving the ester carbonyl) as represented in Figure 1a.^[35] Characterization of **1a** and (*R*)-**2a** mixtures in solution (methylcyclohexane) confirms the aforementioned expectation: **1a** and (*R*)-**2a** are able to stack together through hydrogen bonds between

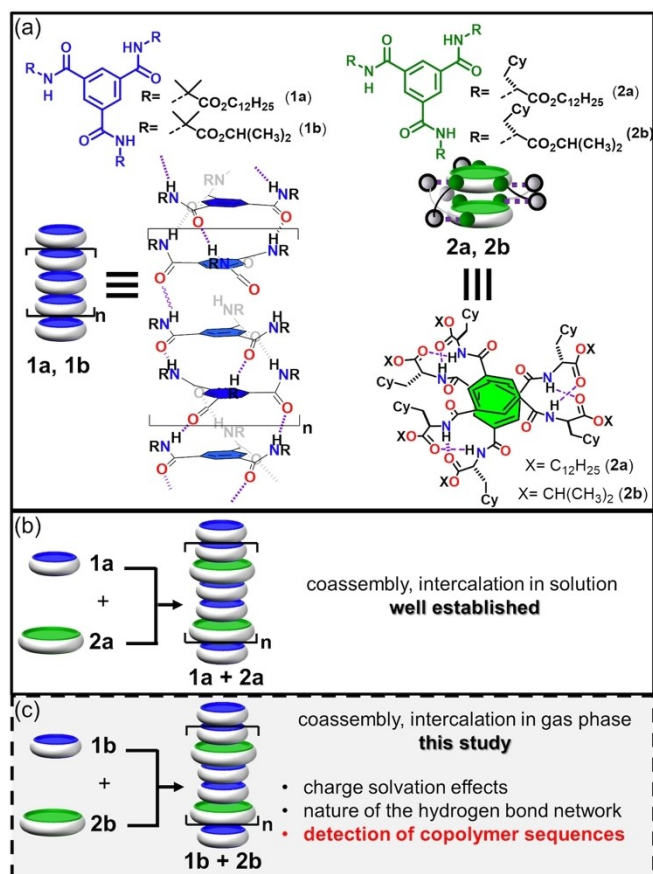


Figure 1. (a) Chemical structure of the BTA monomers used in this study and schematic representation of their self-assemblies. (b) Schematic representation of the co-assemblies formed by mixing **1a** and (*R*)-**2a** in solution. (c) Aim of the present study: characterization of the co-assemblies of **1b** and **2b** in the gas phase.

their amide functions (Figures S1 and S2) yielding helical co-assemblies with a preferred left handedness (Figure 1b).

X-ray determination of the structure of **1b** and (*S*)-**2b** (abbreviated as **2b** in the following) in the crystalline state is consistent with the formation of the same type of assemblies as their dodecyl analogues, i.e. helical stacks and dimers, respectively (Figures S3 and S4).

Homo-Assemblies in the Gas Phase

ESI-MS spectra resulting from analysis of **1b** or **2b** BTA samples show both singly and doubly charged species. In addition, BTA are detected mainly under sodiated forms, along with the presence of adducts with proton, ammonium and potassium to a lesser extent (Figures S5 to S7). Examination of the spectrum of BTA **1b** reveals the presence of monomer to decamer from *m/z* 614.3055 (1+) to 2979.5663 (2+), whereas BTA **2b** is detected almost exclusively as monomer and dimer at *m/z* 818.4920 (1+) and 1613.9983 (1+). These results are perfectly consistent with the fact that BTA **1a** was shown to form long stacks in solution while BTA **2a** was shown to form only dimers (see

above). Switching from MS to IM–MS mode allows a straightforward confirmation of the previous assignments, because isobaric species can be differentiated thanks to ion mobility separation (Figures S8 and S9). However, in this mode, heptamer (**1b**)₇ at *m/z* 2092.5930 is the largest species that can be detected without truncation of the mobility signal (Figure 2, top).

As previously described for peptides, oligorotaxanes, and polymers, monitoring experimental CCS as a function of the number of repeat units is a good way to gain information on the shape of macromolecules.^[23,24,36–43]

Figure 2 (bottom) shows such a plot up to a degree of polymerization (DP) of 7: a good fit was obtained using a linear relationship ($CCS = 73.2 \times DP + 240.5$) which is characteristic of rod-like objects.^[23] These results are in perfect agreement with the fact that BTA **1a** was shown to form long stacks in solution.^[35]

The experimental CCS were then compared to the data extracted from Molecular Dynamics (MD) simulations. The structures of both neutral and disodiated **1b** hexamers, (**1b**)₆ and (**1b**)₆Na₂²⁺, respectively, were considered to evaluate the influence of the sodium ions on the assembly organiza-

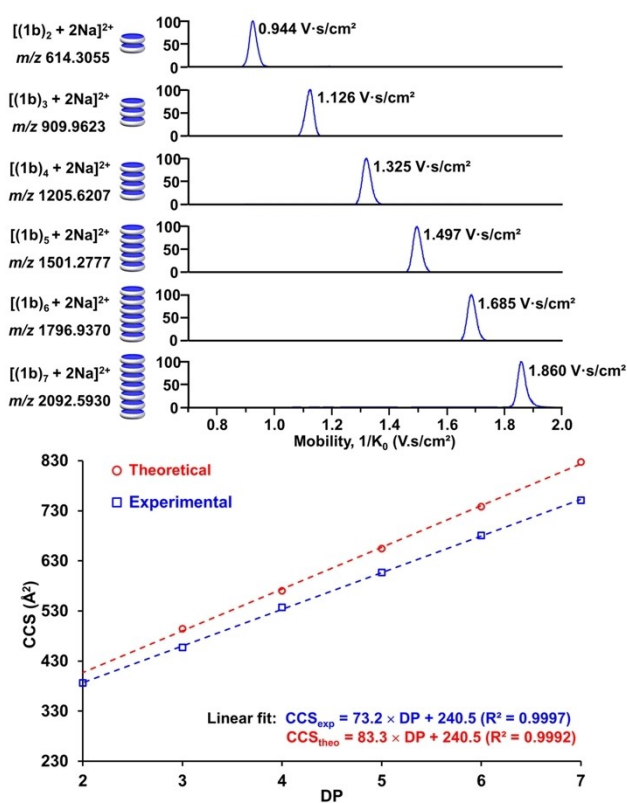


Figure 2. Ion mobility analysis of doubly sodiated **1b** oligomers. Each mass-selected [(**1b**)_{DP} + 2Na]²⁺ ion from ESI-MS yields a mobilitygram with a given mobility value (top). Evolution of experimental (blue square) and theoretical (red circle) average CCS of [(**1b**)_{DP} + 2Na]²⁺ oligomers as a function of the number of monomer units (DP) (bottom). Samples were measured by quintuplicate, and standard deviations for CCS determination were below 0.6%. Mobility values were converted to CCS values using the Mason-Schamp equation for a calibrated TIMS instrument and nitrogen as buffer gas (see SI).

tion. The MD trajectories were first analysed in terms of hydrogen bonds. To evaluate the number of hydrogen bonds, a radial distribution function $g(r)$ was used with a cut-off distance of 2.5 Å as a limit for hydrogen bonds (no angular dependency was thus considered). An ideal assembly constituted of repetitive motifs would have a triple-helix of hydrogen bonds between amide groups where 15 out of 18 amide hydrogens, (i.e. 83 % of them) would be hydrogen-bonded with a neighbouring amide oxygen, and the remaining 3 hydrogens would be free due to unfavourable orientation (they are localized at the stack extremities). For (**1b**)₆, it is actually found that 94 % of the amide hydrogens are involved in hydrogen bonds within a triple-helix network, but when considering the acceptors, the amide oxygens have a contribution of only 76 %. There is thus a contribution of ester oxygens as acceptors. This contribution is 18 % (Figure 3a, bottom), which implies that during the MD run, the ideal assembly built as a starting structure reorganized to maximize the hydrogen-bond network (see Supporting Information for a more detailed analysis of the hydrogen-bond network within the assembly).

When two sodium ions are added to the assembly ((**1b**)₆Na₂²⁺), one of the three helices of hydrogen bonds is no longer maintained, as can be seen in a picture of the assembly (Figure 3b, top) or in the analysis of hydrogen bonds between amide groups belonging to a given helix (Figure 4a). Indeed, two out of three helices have 74 % of bonded hydrogens, a proportion similar to that in the neutral assembly; but the third, disrupted helix has only 15 % of bonded hydrogens (i.e. only one such bond is still present), with a $g(r)$ peak strongly displaced to a larger distance (+0.5 Å), thus reflecting the weakness of the

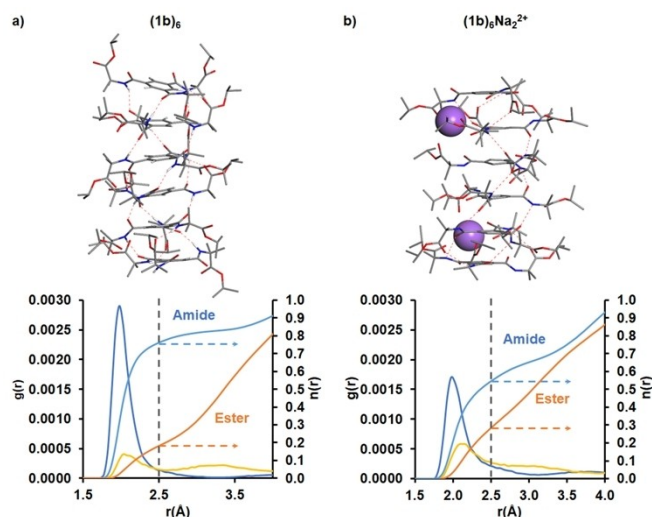


Figure 3. Snapshot of a typical structure obtained during MD (top) and radial distribution function $g(r)$ and cumulative number $n(r)$ of amide hydrogens as a function of the distance from the amide/ester oxygens, as calculated during the equilibrated part of the MD trajectory (bottom) for a) (**1b**)₆ and b) (**1b**)₆Na₂²⁺, respectively. The sodium ions are in violet and the hydrogen bonds are red dotted lines; hydrogen atoms were removed for the sake of clarity. The grey dotted line represents the cut-off distance of 2.5 Å as a limit for hydrogen bonds.

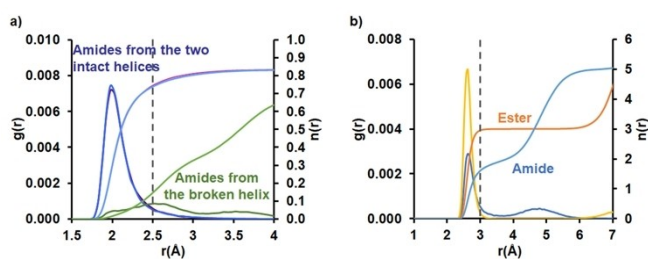


Figure 4. Analysis of the equilibrated part of the MD trajectory of $(\mathbf{1b})_6\text{Na}_2^{2+}$. a) Radial distribution function $g(r)$ and cumulative number $n(r)$ of amide hydrogens as a function of the distance from the amide oxygens. The amides were divided in three categories according to the hydrogen-bond helix to which they belong in $(\mathbf{1b})_6$, i.e. prior to the addition of the sodium ions. Blue and violet curves correspond to intact helices whereas the green curve represents the amide from the broken helix. b) Radial distribution function $g(r)$ and cumulative number $n(r)$ of amide and ester oxygens as a function of the distance from the sodium ions.

interaction (Figure 4a). The addition of sodium ions thus leads to a drop of hydrogen bonds with amide oxygens from 76 % to 54 %. But the contribution of ester oxygens increases from 18 % to 27 % (Figure 3b). As a result, the perturbation induced by the sodium ions has a limited effect on the total number of hydrogen bonds, which drops only from 94 % to 81 %.

Radial distribution functions between amide and ester oxygens on one hand, and sodium ions on the other hand, show a peak corresponding to complexation at 2.6 Å (Figure 4b). For ester, the peak is sharp, with an intensity dropping to almost zero at 3 Å and corresponding to three ester groups. For amide, the peak is broader, probably because the amides being directly grafted to the core have less freedom to organize than the esters (one torsional degree of freedom vs three). At 3.7 Å, the cumulated number of amide oxygens is close to 2. Hence, each sodium is surrounded by three ester oxygens and two amide oxygens (see a picture highlighting the complexing ester/amide oxygens in Figure S20). It is the involvement of amide oxygens in sodium complexation that is partly detrimental to hydrogen-bonding via these atoms. The disodiated assembly is also more compact than that without sodium (compare the two structures in Figure 3). A stack compaction of 3 % is observed at the level of the BTA cores, probably because each sodium clips together one half of the assembly (three neighbouring molecules) by interacting strongly with 5 amide/ester oxygens. The immobilization of mobile ester moieties by the sodium ions also participates to the compaction at the extremities of the assembly. One can conclude from these MD studies that the impact of charge solvation on the one-dimensional stacking in the gas phase is minimal as sodium-oxygen interactions replace part of the hydrogen bonds to glue the molecules.

Based on such optimized structures, the various $\mathbf{1b}$ homo-assemblies have been processed using the Collidscope software^[44] to compute average theoretical CCS (Figure 2). Interestingly, both experimental and theoretical series show a linear trend, having the same ordinate at the

origin (240.5 \AA^2) and similar slopes (83.3 \AA^2 vs 73.2 \AA^2 for theoretical and experimental data, respectively). This confirms the previous interpretation that $\mathbf{1b}$ oligomers form one-dimensional stacks in the gas phase.

Due to the absence of ambiguity about their organization, the homo-assemblies $(\mathbf{1b})_{\text{DP}}\text{Na}_2^{2+}$ can be used as a reference system to correct theoretical CCS, and then be applied to $(\mathbf{1b} + \mathbf{2b})$ copolymer systems. To obtain the best agreement with experimental CCS, a corrected theoretical CCS can be accessed with the following equation:

$$\text{CCS}_{\text{corr}} = \frac{73.2}{83.3} (\text{CCS}_{\text{th}} - 240.5) + 240.5 \quad (1)$$

For oligomers of DP6, which will be studied in more details, this correction is similar to applying a scaling factor of 0.92 to the theoretical CCS.

Sequence of Copolymers in the Gas Phase

A pre-mixed equimolar mixture of $\mathbf{1b}$ and $\mathbf{2b}$ (see experimental section) was investigated by ESI-MS. The resulting spectrum exhibited different series of peaks with m/z values corresponding to DP 2 to 8 with varying composition that are characteristic of the resulting hetero co-assemblies. A careful examination of the spectrum reveals that all possible dimers, trimers, and tetramers were successfully detected (Figure 5). It is worth noting that $(\mathbf{2b})_3$ and $(\mathbf{2b})_4$, which are not detected in the analysis of pure $\mathbf{2b}$, are only minor in $\mathbf{1b}/\mathbf{2b}$ mixture within their DP set (14 and 3 % of all detected DP3 and DP4, respectively) and represent only ~1 % of all assemblies. We assume that they most probably result from slight aggregation during the ESI process because the total BTA concentration is higher in this experiment.

Regarding pentamers and hexamers, all possible compositions were also detected, except $(\mathbf{2b})_5$ and $(\mathbf{2b})_6$, as expected from previous results (see above). The number of peaks ascribed to heptamers and octamers is lower than

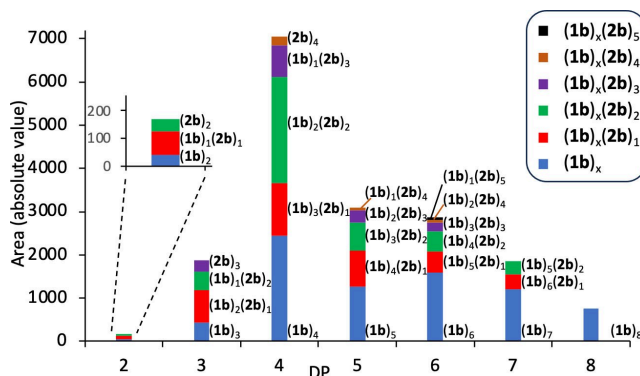


Figure 5. Size and composition distributions of the oligomers detected under disodium adducts for the $\mathbf{1b}/\mathbf{2b}$ 1/1 mixture extracted from IM-MS analysis. For a given oligomer size (DP), the composition is illustrated using different colours according to the inset ($0 \leq x \leq 8$).

expected and is due to the quadrupole-MS transfer settings-based mass range. While this mass spectrum informs us on the composition variations of the oligomers within a given sample, it contains no details on the exact position of the co-monomers within each oligomer. In contrast, IM-MS may reveal such information. To test this approach, firstly the robustness of the data was probed, by repeating five times the analysis of the **1b/2b** 1/1 mixture. All IM peaks corresponding to oligomers were summarized in Table 1.

The results show that as expected, a single peak is detected for each dimer, while up to 3 peaks can be unambiguously distinguished for some longer oligomers (Table 1 and Figures S13 to S18). Interestingly, changing the initial **1b/2b** ratio yielded the same m/z values and CCS for mass spectrum and mobilogram, respectively (Table S2). For example, with the m/z 2001.1237 corresponding to the $[(\mathbf{1b})_4(\mathbf{2b})_2+2\text{Na}]^{2+}$ ion, IM experiments unambiguously highlighted the presence of at least three distinct peaks among the nine that can potentially be encountered (Figure 6). These three structures may correspond to different positions of the co-monomers within the hexamer assembly.

To verify such assumption, and provide sequence information about the various detected mobility peaks, the CCS of all 9 possible sequences were calculated using MD theoretical approach. The theoretical CCS distribution of the nine $(\mathbf{1b})_4(\mathbf{2b})_2\text{Na}_2^{2+}$ co-assemblies (corrected according to Eq. 1) show a strong effect of the nature of the monomers

present at the extremities of the co-assemblies (Figure 6, bottom). The CCS is largest when one molecule of **2b** is present at each extremity (sequence 5). Then, there is a group of four more compact co-assemblies having only one extremity occupied by one molecule of **2b** (sequences 1, 2, 3, and 4). Finally, there is a group of four even more compact co-assemblies having no molecule of **2b** at extremities (sequences 6, 7, 8 and 9). These results are linked to the different size of the monomers, **1b** and **2b**. The largest one, **2b**, has flexible methylcyclohexyl groups that can orient along the axis direction of the co-assemblies when these monomers are present at extremities of the stacks, thus elongating them, which gives rise to larger CCS (Figure S21).

A smaller effect on CCS can also be observed when **2b** is present in penultimate location. In that position, it can also elongate the stack via its methylcyclohexyl groups, though less than when the molecule is directly present at an extremity (see Figure S21, right). In addition, such an effect is manifested only when there is no other molecule of **2b** adjacent at the extremity. When it is the case, the effect is masked by the pre-eminence of the effect produced by the extremal molecule. These reasons explain why structure 4 (one isolated penultimate molecule of **2b**) has a larger CCS than structures 1, 2, and 3 (no isolated penultimate molecule of **2b**), and why structures 6, 7, and 8 (one or two isolated

Table 1: Main average mobility and experimental $\text{TIMS}^{\text{MS}}\text{CCS}_{\text{N}_2}$ values of the doubly sodiated supramolecular oligomers obtained from the **1b/2b** 1/1 mixture. See also Figures S13–S18.

DP ^[a]	Oligomer content	Mobility $1/K_0$ (V.s/cm ²) ^[b]	$\text{TIMS}^{\text{MS}}\text{CCS}_{\text{N}_2}$ (Å ²) ^[c]
2	(1b) ₂	0.942	384.6
	(1b) ₁ (2b) ₁	1.047	426.4
3	(2b) ₂	1.159	470.9
	(1b) ₃	1.122	456.1
	(1b) ₂ (2b) ₁	1.201	487.4
	(1b) ₁ (2b) ₂	1.313	532.2
4	(2b) ₃	1.409	570.3
	(1b) ₄	1.322	535.7
	(1b) ₃ (2b) ₁	1.404	568.4
	(1b) ₂ (2b) ₂	1.464	592.0
	(1b) ₁ (2b) ₃	1.541	622.7 ^[d]
5	(2b) ₄	1.605	648.4
	(1b) ₅	1.496	604.7
	(1b) ₄ (2b) ₁	1.570	634.5
	(1b) ₃ (2b) ₂	1.627; 1.636; 1.657	656.9; 660.4; 669.6
	(1b) ₂ (2b) ₃	1.690; 1.695; 1.705	682.1; 683.9; 687.9
	(1b) ₁ (2b) ₄	1.772	714.7
6	(1b) ₆	1.681	678.3
	(1b) ₅ (2b) ₁	1.741	702.5 ^[d]
	(1b) ₄ (2b) ₂	1.781; 1.796; 1.820	718.3; 724.3; 733.7
	(1b) ₃ (2b) ₃	1.824; 1.839; 1.863	735.3; 741.4; 751.0
	(1b) ₂ (2b) ₄	1.862	750.5 ^[d]
	(1b) ₁ (2b) ₅	1.934; 1.940	779.0; 781.4
7	(1b) ₇	1.856	748.1
	(1b) ₆ (2b) ₁	1.912	770.2
	(1b) ₅ (2b) ₂	1.937; 1.940	780.2; 781.6

[a] DP is the degree of polymerization. [b] Mobility was accessed using elution voltage which is connected to the K_0 value (see SI). Samples were measured by quintuplicate, and standard deviations for CCS determination were below 0.6%. [c] $\text{TIMS}^{\text{MS}}\text{CCS}_{\text{N}_2}$ refers to the determined CCS values using the Mason-Schamp equation for a calibrated TIMS instrument and nitrogen as buffer gas (see SI). [d] This signal is broad.

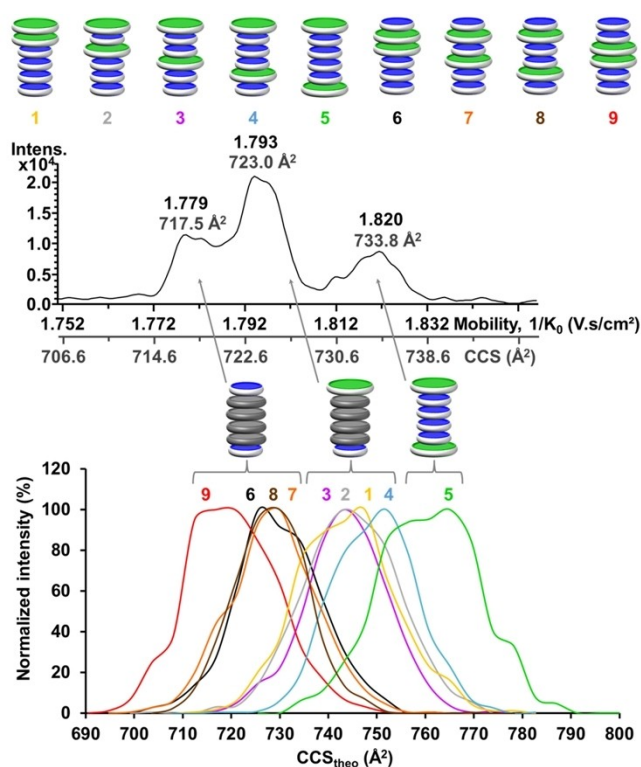


Figure 6. Top) Schematic representation of the nine possible sequence isomers from $(\mathbf{1b})_4(\mathbf{2b})_2$ with $\mathbf{1b}$ as blue disc and $\mathbf{2b}$ as green disc. Middle) Mobilogram of the m/z 2001.1237 corresponding to the $(\mathbf{1b})_4(\mathbf{2b})_2$ hexamers detected under disodium adducts for the $\mathbf{1b}/\mathbf{2b}$ 1/1 mixture. Grey arrows show the proposed assignment, where grey disks remain undefined. Bottom) Population distribution of corrected theoretical CCS for the different sequence isomers of $(\mathbf{1b})_4(\mathbf{2b})_2\text{Na}_2^{2+}$.

penultimate molecule(s) of $\mathbf{2b}$ have a larger CCS than structure 9 (no isolated penultimate molecule of $\mathbf{2b}$).

Although we have not performed the same detailed calculations for the other oligomers, the conclusions derived for $(\mathbf{1b})_4(\mathbf{2b})_2$ hexamers can possibly also apply to oligomers of DP 3 to 6. Indeed, according to our interpretation of the major effect of the presence of $\mathbf{2b}$ at 0, 1 or 2 extremities, heterotrimers could show 2 peaks, tetramers $(\mathbf{1b})_1(\mathbf{2b})_3$ and $(\mathbf{1b})_3(\mathbf{2b})_1$ could show two peaks and tetramer $(\mathbf{1b})_2(\mathbf{2b})_2$ could show 3 peaks. The fact that we detect only one main peak for all of them either means that some sequences are not populated or that trimers and tetramers are too short to allow discrimination of their CCS in our experimental conditions. In the same line, pentamers $(\mathbf{1b})_1(\mathbf{2b})_4$ and $(\mathbf{1b})_4(\mathbf{2b})_1$ and hexamers $(\mathbf{1b})_1(\mathbf{2b})_5$ and $(\mathbf{1b})_5(\mathbf{2b})_1$ are expected to show at most 2 well resolved peaks, and they indeed show either one or two peaks (Table 1). Finally, pentamers $(\mathbf{1b})_2(\mathbf{2b})_3$ and $(\mathbf{1b})_3(\mathbf{2b})_2$ and hexamers $(\mathbf{1b})_2(\mathbf{2b})_4$ and $(\mathbf{1b})_3(\mathbf{2b})_3$ are expected to show at most 3 well resolved peaks, which they do (Tables 1 and S2).

Conclusions

We have demonstrated for the first time that BTA supramolecular polymers can be analysed by IM-MS up to a degree of polymerisation of 7 and that their rigid rod-like conformation is maintained in the gas phase, as indicated by the linear evolution of their CCS. Moreover, in the case of copolymers IM-MS allows to discriminate up to three CCS for a given copolymer composition, indicating the presence of several isomers. Based on theoretical calculations, we propose an assignment for these isomeric structures, where the main effect is the presence of the bulkiest monomer at 0, 1 or 2 extremities. Considering the on-going improvements of instrumental resolution, it can be anticipated that the other isomers will also be resolved in the future. Moreover, although not achievable on our instrument, MS/MS experiments after the ion mobility step should shed more light on the herein investigated copolymers,^[25d-f] by probing the stability of the oligomers as well as by unveiling the identity of the terminal units, where fewer hydrogen bonds are involved. Our study therefore opens the door to the identification and relative quantification of supramolecular copolymer sequences. Moreover, the herein approach could be used to monitor the conformational state and topology of the assemblies.

Supporting Information

The authors have cited additional references within the Supporting Information (Ref. [45–55]).

Acknowledgements

The authors thank the French Ministry of Research and French National Research Agency as part of the MetaboHUB infrastructure for funding (ANR-11-INBS-0010 grant). Research in Mons is supported by the Belgian National Fund for Scientific Research (FRS-FNRS) within the Consortium des Équipements de Calcul Intensif – CÉCI, and by the Walloon Region (LUCIA Tier-1 supercomputer).

Conflict of Interest

The authors declare no conflict of interest.

Data Availability Statement

The data that support the findings of this study are available from the corresponding author upon reasonable request.

Keywords: supramolecular copolymer · sequence · ion mobility · IMMS · benzenetricarboxamide

- [1] J. Matern, Y. Dorca, L. Sánchez, G. Fernández, *Angew. Chem. Int. Ed.* **2019**, *58*, 16730–16740.
- [2] T. F. A. De Greef, M. M. J. Smulders, M. Wolffs, A. P. H. J. Schenning, R. P. Sijbesma, E. W. Meijer, *Chem. Rev.* **2009**, *109*, 5687–5754.
- [3] E. Krieg, M. M. C. Bastings, P. Besenius, B. Rybtchinski, *Chem. Rev.* **2016**, *116*, 2414–2477.
- [4] Y. Li, A. Hammoud, L. Bouteiller, M. Raynal, *J. Am. Chem. Soc.* **2020**, *142*, 5676–5688.
- [5] A. Desmarchelier, X. Caumes, M. Raynal, A. Vidal-Ferran, P. W. N. M. van Leeuwen, L. Bouteiller, *J. Am. Chem. Soc.* **2016**, *138*, 4908–4916.
- [6] J. M. Zimbron, X. Caumes, Y. Li, C. M. Thomas, M. Raynal, L. Bouteiller, *Angew. Chem. Int. Ed.* **2017**, *56*, 14016–14019.
- [7] R. Chen, A. Hammoud, P. Aoun, M. A. Martínez-Aguirre, N. Vanthuyne, R. Maruchenko, P. Brocorens, L. Bouteiller, M. Raynal, *Nat. Commun.* **2024**, *15*, 4116, <https://www.nature.com/articles/s41467-024-48412-z>.
- [8] B. Adelizzi, P. Chidchob, N. Tanaka, B. A. G. Lamers, S. C. J. Meskers, S. Ogi, A. R. A. Palmans, S. Yamaguchi, E. W. Meijer, *J. Am. Chem. Soc.* **2020**, *142*, 16681–16689.
- [9] M. H. Bakker, C. C. Lee, E. W. Meijer, P. Y. W. Dankers, L. Albertazzi, *ACS Nano* **2016**, *10*, 1845–1852.
- [10] J.-F. Lutz, M. Ouchi, D. R. Liu, M. Sawamoto, *Science* **2013**, *341*, 1238149, <https://www.science.org/doi/10.1126/science.1238149>.
- [11] A. Sorrenti, J. Leira-Iglesias, A. J. Markvoort, T. F. A. de Greef, T. M. Hermans, *Chem. Soc. Rev.* **2017**, *46*, 5476–5490.
- [12] D. Görl, X. Zhang, V. Stepanenko, F. Würthner, *Nat. Commun.* **2015**, *6*, 7009, <https://www.nature.com/articles/ncomms8009>.
- [13] A. Sarkar, R. Sasmal, A. Das, A. Venugopal, S. S. Agasti, S. J. George, *Angew. Chem. Int. Ed.* **2021**, *60*, 18209–18216.
- [14] G. B. W. L. Ligthart, H. Ohkawa, R. P. Sijbesma, E. W. Meijer, *J. Am. Chem. Soc.* **2005**, *127*, 810–811.
- [15] S. M. Waybright, C. P. Singleton, K. Wachter, C. J. Murphy, U. H. F. Bunz, *J. Am. Chem. Soc.* **2001**, *123*, 1828–1833.
- [16] R. Takasawa, K. Murota, I. Yoshikawa, K. Araki, *Macromol. Rapid Commun.* **2003**, *24*, 335–339.
- [17] B. Adelizzi, N. J. Van Zee, L. N. J. De Windt, A. R. A. Palmans, E. W. Meijer, *J. Am. Chem. Soc.* **2019**, *141*, 6110–6121.
- [18] A. Sarkar, T. Behera, R. Sasmal, R. Capelli, C. Empereur-mot, J. Mahato, S. S. Agasti, G. M. Pavan, A. Chowdhury, S. J. George, *J. Am. Chem. Soc.* **2020**, *142*, 11528–11539.
- [19] L. N. J. De Windt, C. Kulkarni, H. M. M. Ten Eikelder, A. J. Markvoort, E. W. Meijer, A. R. A. Palmans, *Macromolecules* **2019**, *52*, 7430–7438.
- [20] H. M. M. Ten Eikelder, A. J. Markvoort, *Acc. Chem. Res.* **2019**, *52*, 3465–3474.
- [21] L. N. J. Windt, Z. Fernández, M. Fernández-Míguez, F. Freire, A. R. A. Palmans, *Chem. Eur. J.* **2022**, *28*, e202103691, <https://chemistry-europe.onlinelibrary.wiley.com/doi/full/10.1002/chem.202103691>.
- [22] B. Adelizzi, A. Aloï, A. J. Markvoort, H. M. M. Ten Eikelder, I. K. Voets, A. R. A. Palmans, E. W. Meijer, *J. Am. Chem. Soc.* **2018**, *140*, 7168–7175.
- [23] J. R. N. Haler, E. Béchet, C. Kune, J. Far, E. De Pauw, *J. Am. Soc. Mass Spectrom.* **2022**, *33*, 273–283.
- [24] S. Hoyas, E. Halin, V. Lemaur, J. De Winter, P. Gerbaux, J. Cornil, *Biomacromolecules* **2020**, *21*, 903–909.
- [25] a) L. Charles, C. Chendo, S. Poyer, *Rapid Commun. Mass Spectrom.* **2020**, *34*, e8624, <https://doi.org/10.1002/rcm.8624>; b) Q. Duez, S. Hoyas, T. Josse, J. Cornil, P. Gerbaux, J. De Winter, *Mass Spectrom. Rev.* **2023**, *42*, 1129–1151; For the use of IM–MS to detect sequence isomers in covalent copolymers see: c) E. S. Baker, J. Gidden, W. J. Simonsick, M. C. Grady, M. T. Bowers, *Int. J. Mass Spectrom.* **2004**, *238*, 279–286; d) N. E. Alexander, J. P. Swanson, A. Joy, C. Wesdemiotis, *Int. J. Mass Spectrom.* **2018**, *429*, 151–157; e) A. P. Gies, D. M. Hercules, *Anal. Chim. Acta* **2014**, *808*, 199–219; f) Q. Duez, S. Moins, O. Coulembier, J. De Winter, J. Cornil, P. Gerbaux, *J. Am. Soc. Mass Spectrom.* **2020**, *31*, 2379–2388.
- [26] M. M. Zimnicka, *Mass Spectrom. Rev.* **2023**, mas.21851, <https://doi.org/10.1002/mas.21851>.
- [27] E. Kalenius, M. Groessl, K. Rissanen, *Nat. Chem. Rev.* **2019**, *3*, 4–14, <https://doi.org/10.1038/s41570-018-0062-2>.
- [28] A. Kiesilä, L. Kivijärvi, N. K. Beyeh, J. O. Moilanen, M. Groessl, T. Rothe, S. Götz, F. Topić, K. Rissanen, A. Lützen, E. Kalenius, *Angew. Chem. Int. Ed.* **2017**, *56*, 10942–10946.
- [29] N. Geue, R. E. P. Winpenny, P. E. Barran, *J. Am. Chem. Soc.* **2024**, *146*, 8800–8819, <https://pubs.acs.org/doi/10.1021/jacs.4c00354>.
- [30] M. C. Pfrunder, D. L. Marshall, B. L. J. Poad, T. M. Fullon, J. K. Clegg, S. J. Blanksby, J. C. McMurtrie, K. M. Mullen, *Angew. Chem. Int. Ed.* **2023**, *62*, e202302229, <https://doi.org/10.1002/anie.202302229>.
- [31] K. J. Endres, K. Barthelmes, A. Winter, R. Antolovich, U. S. Schubert, C. Wesdemiotis, *Rapid Commun. Mass Spectrom.* **2020**, *34*, e8717, <https://doi.org/10.1002/rcm.8717>.
- [32] C. Bleiholder, N. F. Dupuis, T. Wyttenbach, M. T. Bowers, *Nat. Chem.* **2011**, *3*, 172–177.
- [33] Y. Li, L. Bouteiller, M. Raynal, *ChemCatChem* **2019**, *11*, 5212–5226.
- [34] H. Kong, Y. Li, A. Hammoud, L. Dubreucq, C. Troufflard, R. Maruchenko, L. Bouteiller, M. Raynal, *ChemistryEurope* **2023**, *1*, e202300027, <https://doi.org/10.1002/ceur.202300027>.
- [35] A. Desmarchelier, B. G. Alvarenga, X. Caumes, L. Dubreucq, C. Troufflard, M. Tessier, N. Vanthuyne, J. Ide, T. Maistriaux, D. Beljonne, P. Brocorens, R. Lazzaroni, M. Raynal, L. Bouteiller, *Soft Matter* **2016**, *12*, 7824–7838.
- [36] E. Hanozin, B. Mignolet, J. Martens, G. Berden, D. Sluysmans, A. Duwez, J. F. Stoddart, G. Eppe, J. Oomens, E. De Pauw, D. Morsa, *Angew. Chem. Int. Ed.* **2021**, *60*, 10049–10055.
- [37] S. Hoyas, P. Weber, E. Halin, O. Coulembier, J. De Winter, J. Cornil, P. Gerbaux, *Biomacromolecules* **2021**, *22*, 3543–3551.
- [38] J. R. N. Haler, D. Morsa, P. Lecomte, C. Jérôme, J. Far, E. De Pauw, *Methods* **2018**, *144*, 125–133.
- [39] Q. Duez, T. Josse, V. Lemaur, F. Chiro, C. M. Choi, P. Dubois, P. Dugourd, J. Cornil, P. Gerbaux, J. De Winter, *J. Mass Spectrom.* **2017**, *52*, 133–138.
- [40] E. Hanozin, D. Morsa, E. De Pauw, *J. Phys. Chem. A* **2019**, *123*, 8043–8052.
- [41] E. Hanozin, B. Mignolet, J. Martens, G. Berden, D. Sluysmans, A.-S. Duwez, J. F. Stoddart, G. Eppe, J. Oomens, E. De Pauw, D. Morsa, *Angew. Chem. Int. Ed.* **2021**, *60*, 10049–10055.
- [42] E. Hanozin, B. Mignolet, D. Morsa, D. Sluysmans, A.-S. Duwez, J. F. Stoddart, F. Remacle, E. De Pauw, *ACS Nano* **2017**, *11*, 10253–10263.
- [43] Q. Duez, T. Josse, V. Lemaur, F. Chiro, C. M. Choi, P. Dubois, P. Dugourd, J. Cornil, P. Gerbaux, J. De Winter, *J. Mass Spectrom.* **2017**, *52*, 133–138.
- [44] S. A. Ewing, M. T. Donor, J. W. Wilson, J. S. Prell, *J. Am. Soc. Mass Spectrom.* **2017**, *28*, 587–596.
- [45] P. Jana, A. Paikar, S. Bera, S. K. Maity, D. Haldar, *Org. Lett.* **2014**, *16*, 38–41.
- [46] X. Caumes, A. Baldi, G. Gontard, P. Brocorens, R. Lazzaroni, N. Vanthuyne, C. Troufflard, M. Raynal, L. Bouteiller, *Chem. Commun.* **2016**, *52*, 13369–13372.
- [47] A. Hammoud, Y. Li, M. A. Martínez-Aguirre, H. Kong, L. Dubreucq, C. Troufflard, L. Bouteiller, M. Raynal, *Chem. Eur.*

- J.* **2023**, *29*, e202300189, <https://doi.org/10.1002/chem.202300189>.
- [48] A. Desmarchelier, M. Raynal, P. Brocorens, N. Vanthuyne, L. Bouteiller, *Chem. Commun.* **2015**, *51*, 7397–7400.
- [49] S. L. Mayo, B. D. Olafson, W. A. Goddard III., *J. Phys. Chem.* **1990**, *94*, 8897–909.
- [50] S. Hoyas, V. Lemaury, Q. Duez, F. Saintmont, E. Halin, J. De Winter, P. Gerbaux, J. Cornil, *Adv. Theory Simul.* **2018**, *1*, 1800089, <https://doi.org/10.1002/adts.201800089>.
- [51] H. Sun, *Macromolecules* **1995**, *28*, 701–12.
- [52] H. Sun, *J. Comput. Chem.* **1994**, *15*, 752–68.
- [53] S. Nose, *Mol. Phys.* **1984**, *52*, 255–68, <https://doi.org/10.1080/00268978400101201>.
- [54] L. Verlet, *Phys. Rev.* **1967**, *159*, 98–103.
- [55] M. P. Lightfoot, F. S. Mair, R. G. Pritchard, J. E. Warren, *Chem. Commun.* **1999**, 1945–1946.

Manuscript received: November 3, 2024

Accepted manuscript online: January 22, 2025

Version of record online: February 5, 2025